Journal of Materials Chemistry A

Accepted Manuscript

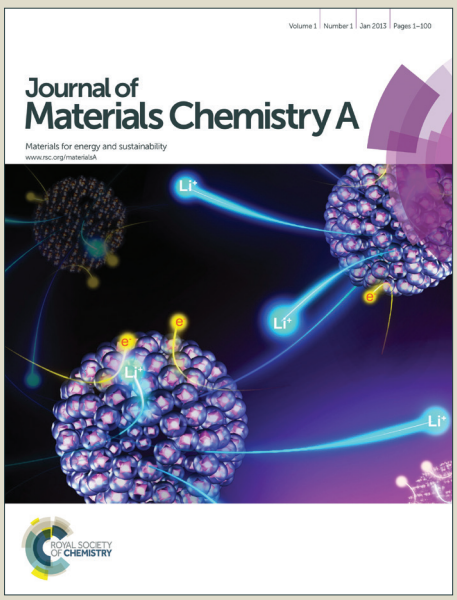

ROYAL SOCIETY OF CHEMISTRY

www.rsc.org/materialsA

ToC

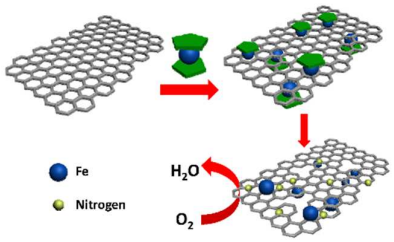

Ferrocene was utilized to functionalize reduced graphene oxide and exfoliate graphite flake by ligand-exchange reaction.

Journal Name

RSCPublishing

ARTICLE

Efficient Approach to Iron/Nitrogen co-Doped Graphene Materials as Efficient Electrochemical Catalysts for Oxygen Reduction Reaction

Cite this: DOI: 10.1039/x0xx00000x

Received 00th January 2012,
Accepted 00th January 2012

DOI: 10.1039/x0xx00000x

www.rsc.org/

Qingqing Dong[a,b†], Xiaodong Zhuang[b†], Zhi Li[a*], Bin Li[a*], Bin Fang[a], Cunzhong Yang[a], Haifen Xie[a], Fan Zhang[b]*, Xinliang Feng[b,c]

Cyclopentadienyliron (CpFe) groups have been successfully attached on the surfaces of reduced graphene oxide (rG) by a ligand-exchange reaction of ferrocene (Cp2Fe) and rG, to produce CpFe-modified reduced graphene oxide (rGFeCp), which exhibits good processability in many organic solvents. In a similar one-pot performance, the graphite was efficiently exfoliated using Cp2Fe as the intercalators, to form CpFe-attached free-standing graphene nanosheets (GFeCp, ~10 layers). Upon pyrolysis and ammonia activation, rGFeCp and GFeCp were converted to iron/nitrogen co-doped porous graphenes, rGFe-800a and GFe-800a, respectively. The obtained rGFe-800a exhibited good electrochemical performance for oxygen reduction reaction (ORR) under alkaline condition (0.1 M KOH), with a low half-wave potential at -0.29 V, a dominant four-electron transfer mechanism (n=3.5 at -1.0 V), and a maximum diffusion-limiting current density of 4.86 mAcm-2. In addition, it showed excellent methanol tolerance, superior to commercial 20% Pt/C. The effect of iron/nitrogen co-doping serves as the key role in the good ORR activities of the as-prepared materials.

Introduction

Graphene, since found in 2004, has led to an explosion of interest due to its prominent properties and broad potential applications in many fields.[1] Its single-layer two-dimensional structure accompanied with high surface area render it suitable for building up nanostructured hybrid materials[2,3]. In particular, the worldwide consciousness of the sustainable low-carbon economy greatly promotes the development of graphene-based new energetic materials.[4-7] The electrochemically catalyzed oxygen reduction reaction (ORR) is an important process in fuel cells and metal-air batteries.[8,9] Since platinum-based materials have the highest catalytic activities for oxygen reduction among most of the pure metals supported on conductive carbons, they serve as state-of-art cathode materials in low-temperature fuel cells.[10,11] However, large-scale production for such kind of precious metal-containing catalysts is impossible because of the stiff price and the scarcity of Pt.[12] On the other hand, Pt-based catalysts are unfavorable for the endurance test due to their sensitive to CO and methanol. Hence, finding an inexpensive material to replace platinum is extremely important for the widespread application of fuel cells.[13] In this aspect, heteroatom-doped (such as S, P and N) graphenes possess several potential advantages. Typically, nitrogen has proven to be an efficient dopant to greatly improve the activity and stability of the graphene-based ORR catalysts[14], through creating electrically non-neutral sites on the graphene surface.[15-19] A variety of non-noble metals compounds, such as transition-metal oxides/chalcogenides[20,21], have also been used to form metal-doped graphene composites, exhibiting very good electrochemical performance in ORR catalysis,[22] because these compounds can serve as separators for tuning the interplanar spacing of the neighboring graphene sheets, and essentially allowing both sides of each graphene sheet for accessible to the electrolyte. Despite the uniform functionalization of carbon black or carbon nanotubes with transition metal (e.g. Fe) has become extremely successful, however, it is still a big challenge for graphene due to the limited preparation strategies [23-27].

Our present task focused on exploring new method for efficiently codoping heteroatom and transition-metal in graphene. Given that reduced graphene oxide (rG) is one of the most easily-available derivatives of graphene featuring good conductivity and large specific surface area, hereby we report a new synthetic method for the formation of cyclopentadienyliron (CpFe) modified rG (rGFeCp), and CpFe modified few-layer graphene nanosheets (GFeCp), by the convenient ligand-exchange reactions of ferrocene with rG and graphite, respectively. The as-prepared rGFeCp or GFeCp was further pyrolyzed under nitrogen, and activated under ammonia at different temperatures to produce a series of graphene composites with high nitrogen/iron doping contents (the highest values are N: 2.94 at% and Fe: 1.84 at%). The resulting materials exhibited porous structures and sheet-like morphologies. They enable undergoing ORR catalysis in alkaline, with good performance (e.g. primary four electron transfer mechanism) comparable with that of the commercial Pt/C catalyst.[28,29]

Results and discussion

The strategy for the synthesis of iron/nitrogen co-doped porous graphene nansheets (rGFe-800a) is presented in Figure 1. According to the typical organometallic ligand-exchange reaction[30] of polyaromatic molecules and ferrocene as reported in 1974,

cyclopentadienyliron (CpFe) has been successfully attached on carbon nanotubes[23], carbon black and highly oriented pyrolytic graphite[31] due to the large amount of the six-membered phenyl ring on the surfaces of these materials. Similarly, in our present work, CpFe substituted graphene rGFeCp was readily obtained by the reaction of reduced graphene oxide (rG) and ferrocene in anhydrous cyclohexane in presence of Al/$AlCl_3$. Upon pyrolysis and ammonia activation at 800 ^oC, the resulting rGFeCp can be easily converted into the nitrogen/iron co-doped porous graphene rGFe-800a. For comparison, iron/nitrogen co-doped porous graphite (GFe-800a) was also prepared under the similar reaction conditions, by using graphite as starting material instead of rG. Certainly, such a concise preparation approach using low-cost ferrocene and ammonia as iron and nitrogen sources, respectively, make it possible to produce rGFe-800a in large scale, and further explore its practical applications in a wide range.

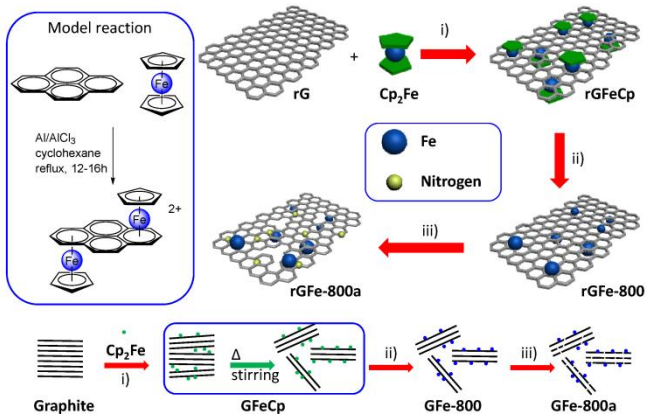

Figure 1. Preparation of cyclopentadienyl iron functionalized reduced graphene oxide/graphite by ligand exchange reaction (hydrated Al anions are omitted for clarity). (i) Al, $AlCl_3$, cyclohexane, 80 ℃, 36 h; (ii) 800 ℃, N_2, 2 h; (iii) 800 ℃, NH_3, 10 min.

Obviously, after the ligand-exchange reaction, one of the Cp ligands of each ferrocene molecule was took place by the unsaturated unit (e.g. benzene ring) in the graphene layer, leading to a CpFe moiety covalently bonding to the surface of rG through the interaction of iron atom with the π-electron of rG.[30] Upon such an attaching mode, a large amount of CpFe units can be efficiently loaded on the both sides of graphene layers, to form sandwich-type rGFeCp composites. The morphology and microstructure of the as-prepared materials were investigated by scanning electron microscopy (SEM), transmission electron microscopy (TEM), and atomic force microscopy (AFM). As shown in Figure 2a, the free-standing nanosheets with the sizes ranging from 250 nm to several micrometers were observed. In addition, rGFeCp also exhibited wrinkles (Figure 2b) similar to that of rGO. The enlarged TEM image shows typical roughness similar to those of previous reports about functionalized graphene oxide.[32,33] We further conducted the similar ligand-exchange performance for exfoliation of graphite. After stirring the mixture of ferrocene and graphite flakes in organic solvents, e.g. DMF, THF or NMP et al, for 36 hours, a large amount of free-standing graphene nanosheets (GFeCp) with good dispersibility in these solvents were formed probably due to the attachment of the CpFe moieties on the surface of the graphene sheets (Figure 2d-f and Figure S2). After collected by centrifugation, we found that most of the nanosheets are consisting of less than ten layers of graphene with the thickness around 17 nm ((Figure 2g, Figure S1). Such an approach offers a facile way to exfoliation of graphite and meanwhile formation of CpFe-modified graphenes. Attempt to achieve high-quality graphene with single or few layers by optimizing the performance is under way.

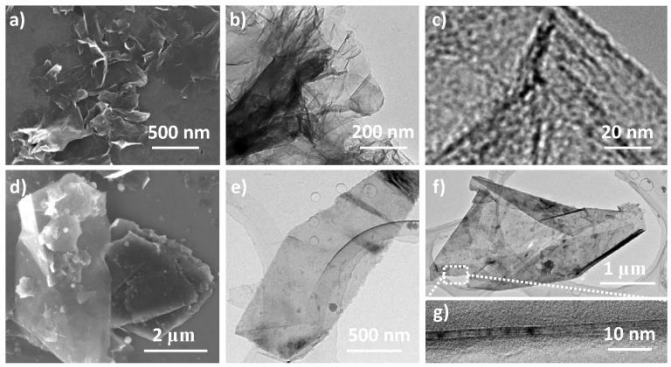

Figure 2. SEM (a) and TEM (b, c) of rGFeCp, and SEM (d) and TEM (e-g) of GFeCp.

To make an insight into the chemical structure of rGFeCp and GFeCp, fourier transform infrared (FT-IR), Raman spectroscopy and X-ray photoelectron spectroscopy (XPS) were employed (Figure 3). In the FT-IR spectra (Figure 3a), the transmittance peaks at 1407 cm^{-1} and 1635 cm^{-1} indicated the presence of the aromatic C=C stretch for both rGFeCp and GFeCp. The peak at around 1100 cm^{-1} confirms the existence of the iron atoms covalently bonding to the-aromatic ring on the graphene/graphite sheets for both cases.[24] Raman spectroscopy has been widely used to characterize the structure of carbon materials, particularly the defects and the degree of ordering of carbon.[34] The Raman spectra of graphite, ferrocene, GFeCp, rGFeCp and rG were shown in Figure 3b. There are two prominent peaks at 1342 and 1587 cm^{-1}, corresponding to the D and G bands, respectively. As is known, the G band is related to the E_{2g} vibration mode of sp^2 carbon domains, which can be used to explain the degree of graphitization, while the D band is associated with structural defects and partially disordered structures of sp^2 domains. The intensities of the D bands in rGFeCp and GFeCp are lower than those of rG and graphite, respectively, manifesting that partial sp^2 domains were restored at different levels after the ligand-exchange reaction.[34] Obviously, the CpFe moieties on the surface of the rG or graphene sheets provide buffers between graphene layers, and thus suppressing their deformation, and lowering the defect density.[35]

XPS analyses were also conducted for the characterization of the samples of Cp_2Fe, GFeCp and rGFeCp. Fe2p XPS spectra of ferrocene and rGFeCp were shown in Figure 4a and 4b, respectively (Also see Figure S3 in SI). The Fe2p3/2 peak was observed at 707.87 eV, which is similar to that of ferrocene (707.84 eV). The Fe2p spectrum of rGFeCp can be deconvoluted into four peaks at 710.6, 714.2, 722.8, and 724.5 eV. The photoelectron peaks at 724.5 eV correspond to the binding energies of 2p1/2 of Fe(III) and Fe(II) ion,[36] and the peaks at 722.8 eV can be assigned to the binding energies of 2p1/2 of Fe(II) ion.[37] The peaks at 714.2 eV and 710.6 eV are attributed to the 2p3/2 of Fe(II) ion and Fe(III) ion, respectively. In comparison to those peaks of ferrocene, we found that the binding energy was moved to higher levels after ligand exchange, which indicated highly efficient functionalization of cyclopentadienyl iron onto the graphene surfaces. These characterizations clearly confirmed that the CpFe moieties have been successfully attached on the surface of rG or graphites in the as-prepared materials through the suggested bonding mode.

Pyrolysis of carbon-backbone materials under ammonia is usually taken advantage of forming the nitrogen-doped materials with high conductivity and porosity. The as-prepared rGFeCp or GFeCp was firstly pyrolyzed under nitrogen flow at 800 ℃ for 2 h to produce

iron-doped graphene (rGFe-800), which was further converted to iron/nitrogen co-doped porous graphene (rGFe-800a) after activation under ammonia gas at 800 ℃ for 15 min. In order to examine the elemental composition and iron/nitrogen bonding configurations in GFe-800a and rGFe-800a, XPS analyses of these samples were firstly carried out. Fe2p XPS spectra of rGFe-800 and rGFe-800a revealed that the most intense doublet with binding energies of 713.0 eV (Fe 2p1/2) and 725.6 eV (Fe2p3/2) was attributed to Fe(II) (Figure 4c and 4d). After ammonia activation, the new peaks at 710.9 eV (Fe2p1/2) and 724.4 eV (Fe2p3/2) may be attributed to Fe-N bonds.

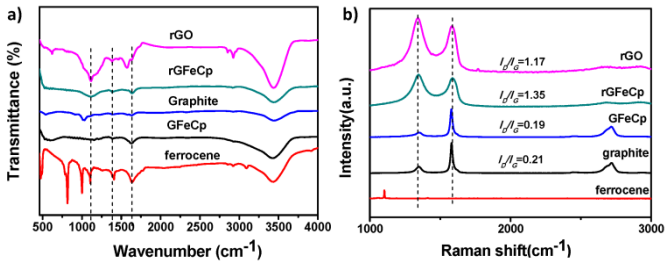

Figure 3. FT-IR spectra (a) and Raman spectra (b) of GFeCp, rGFeCp, graphite, rGO and ferrocene.

Table 1. Nitrogen physisorption properties of rG, rGFeCp, rGFe-700, rGFe-800, rGFe-900 and rGFe-800a.

	S_{BET} [a] (m^2/g)	$S_{langmuir}$ [b] (m^2/g)	D_{av} [c] (nm)	V_{tot} [d] (cm^3/g)
rG	80.2	234.8	1.76	0.35
rGFeCp	36.0	61.4	4.07	0.37
rGFe-700	60.8	115.8	2.26	0.34
rGFe-800	57.5	99.1	14.2	0.41
rGFe-900	87.6	163.4	2.59	0.57
rGFe-800a	57.9	105.8	9.50	0.28

Surface areas calculated from the N_2 adsorption isotherm using the a) BET method and b) Langmuir method; c) Average pore size based on the adsorption isotherm; d) Total pore volume at $p/p_0 = 0.99$.

The bonding configurations of nitrogen in GFe-800a and rGFe-800a were revealed by the N1s core level spectra (Figure 4e and 4f). Both of the nitrogen spectra can be fitted into four types: pyridinic nitrogen (N1, 398.3 eV), pyrrolic nitrogen (N2, 399.8 eV, or Fe-N), graphitic nitrogen (N3, 401.1 eV), and pyridine-N-oxide (N4, 402.7 eV),[34] and all play roles in the ORR process.[38] The peaks with lower binding energy located at about 398.3 eV and 399.8 eV, can be contributed to pyridinic nitrogen (N1), and pyrrolic nitrogen (N2, 399.8 eV, or Fe-N), respectively, of which a pair of *p*-electrons are in the π-conjugated system of the graphene layers. When carbon atoms within the graphene layers were substituted by nitrogen atoms in the form of "graphitic" nitrogen (N3), the corresponding peak in the high-resolution N1s spectra is located at 400.8-401.3 eV. The high energy peak at 402.3-402.9 eV was commonly attributed to oxidized nitrogen of pyridine-N-oxide (N4).[34] As shown in the N1s spectra, N1 and N2 are the main components in GFe-800a (Figure 4e). However, N2 and N3 become predominant for rGFe-800a (Figure 4f). The overall nitrogen contents of GFe-800a and rGFe-800a are 1.07 at% and 2.91 at%, respectively. The results demonstrate that ammonia activation can effectively modulate the chemical states of the nitrogen atoms doped in graphene.

The oxygen reduction reaction (ORR) is of great importance in fuel cells and other electrochemical devices.[39] Recently, great efforts have been focused on developing graphene-based materials for effective and low-cost ORR electrocatalysts.[38,40] In this respect, the as-prepared materials were examined as electrode materials for ORR catalsis. At first, their ORR catalytic activities were first evaluated by cyclic voltammetry (CV) (Figure 5a). The same amount of each sample by mass (0.6 mg/cm^2) was loaded onto a glassy-carbon rotating-disk electrode (RDE). As shown in Figure S4, with an increase in the pyrolysis temperature from 700 to 900 ℃, the onset potentials of rGFe-700, rGFe-800 and rGFe-900 are -0.18 V, -0.14 V and -0.12 V, respectively. rGFe-800 shows the lowest onset potential at -0.12 V and the relatively high diffusion-limiting current density maximum of 5.3 mAcm^{-2}. Featureless voltammetric currents within the potential range between -1.0 V and 0 V were observed for rGFe-800a and GFe-800a in the nitrogen-saturated solution, but the obvious cathodic peaks appeared at -0.25 V and -0.34 V, respectively, when the electrolyte solutions were saturated with O_2, (Figure S5), which suggests the pronounced electrocatalytic activities of rGFe-800a and GFe-800a for oxygen reduction. To examine possible crossover effects, we measured the electrocatalytic selectivity of rGFe-800a and GFe-800a against the electrooxidation of methanol (a common fuel molecule) in O_2-saturated 0.1 M KOH in the presence of methanol (1.0 M). No noticeable changes were observed in the oxygen-reduction currents for these materials (Figure 5a). Thus, either rGFe-800a or GFe-800a exhibited high selectivity for ORR with a remarkably good ability to avoid crossover effects, and thus the as-prepared materials hold a high promise for the utilizations in direct methanol and alkaline fuel cells.

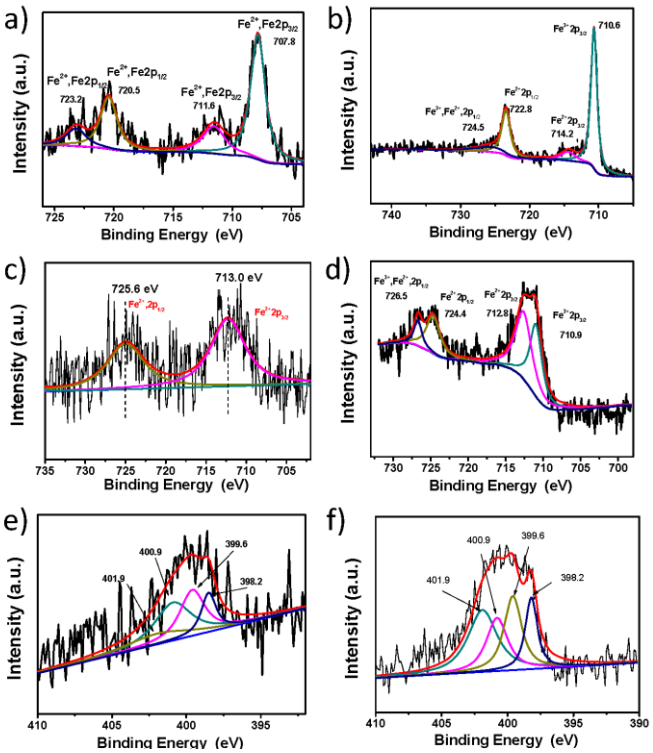

Figure 4. Fe2p XPS spectra of ferrocene (a), rGFeCp (b), rGFe-800 (c), and rGFe-800a (d) and N1s XPS spectra of GFe-800a (e) and rGFe-800a (f).

To gain further understanding the role of rGFe-800a during the ORR electrochemical process, we studied the reaction kinetics by rotating-disk voltammetry. The onset potential for rGFe-800a in RRDE voltammograms was at approximately -0.10 V (Figure 6b), which is close to that identified from CV measurements (-0.11 V, Figure 6a). The calculated electron transfer number and H_2O_2 concentration are 3.5 and ~23% at 1.0 V *vs*. Ag/AgCl (Figure 6c) respectively, which indicate the mainly direct oxygen to water transformation under the catalysis of rGFe-800a. However, the onset potential for GFe-800a (Figure S5) in RRDE voltammograms was at

approximately -0.18 V. The voltammetric profiles in O_2-saturated 0.1 M KOH as the electrolyte showed that the current density was enhanced by an increase in the rotation rate (from 400 to 2500 rpm; Figure 6d). The corresponding Koutecky-Levich plots (Figure 6e) at various electrode potential exhibits good linearity. The slopes remain approximately constant over the potential range from -0.5 V to -1.0 V, which suggests that the electron transfer numbers for oxygen reduction at different electrode potentials are similar. The n was calculated to be 3.83 at -0.25 V. In contrast, the calculated n for GFe-800a was only 2.58 at -0.91 V, and the corresponding Koutecky-Levich plots of GFe-800a at various electrode potential exhibit relatively poor linearity. This result suggests that rGFe-800a leads to a four-electron transfer in oxygen reduction. The calculated kinetic limiting currents for GFe-800a and rGFe-800a reached 13.1 and 15.7 $mAcm^{-2}$, respectively, which are much higher than those of GFe-800 (3.3 $mAcm^{-2}$) and rGFe-800 (9.2 $mAcm^{-2}$).

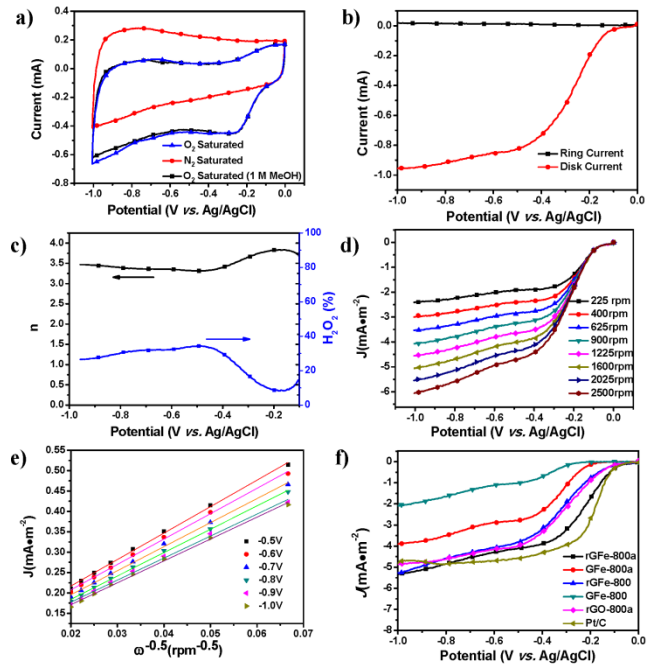

Figure 5. (a) Typical cyclic voltammograms for rGFe-800a at a scan rate of 100 mVs^{-1} in O_2 and N_2-saturated 0.1 M KOH solution as well as in O_2-saturated 0.1 M KOH solution with 1.0 M methanol. (b) RRDE voltammogram for rGFe-800a in 0.1 M KOH solution saturated with O_2; the electrode rotation rate was 1600 rpm, and the Pt ring electrode was held at 0.5 V. (c) Electron transfer number and the percentage of H_2O_2 as a function of potential. (d) RDE voltammograms for rGFe-800a in 0.1 M KOH solution saturated with O_2. (e) Koutecky–Levich plots calculated from the RDE result. (f) Oxygen reduction polarization curves for GFe-800, GFe-800a, rGFe-800, rGFe-800a, rG-800a and Pt/C on GC electrodes at 1600 rpm in 0.1 M KOH.

The corresponding LSV curves for the carbonized samples and Pt/C in an O_2-saturated 0.1 M KOH solution at a rotation rate of 1600 rpm were compared in Figure 5f. The onset potential for rGFe-800, GFe-800a, GFe-800 and Pt/C are -0.09 V, -0.17 V, -0.25 V and -0.087 V, respectively. rGFe-800a shows the highest current density maximum of 4.86 $mAcm^{-2}$. Meanwhile, rGFe-800a has a lowest half-wave potential of -0.29 V and a relatively low onset potential of 0.10 V, which was only 13 mV lower than that of Pt/C (-0.087 V). Therefore, rGFe-800a exhibited better electrocatalytic properties towards ORR than GFe-800a. The concentration of pyrrolic N and graphitic N in rGFe-800a is 67.3 at%, and much lower in GFe-800a (45.7 at%). This suggests that the pyrrolic N and graphitic N may make great contributions to the ORR catalytic activity.[34] Recently, Kim et al. proposed that N-doped edge structures, in particular graphitic N sites, provided the most pronounced improvement for ORR activity,[41] because the relative electronegativity of graphitic N atoms reduces the electron density on the adjacent C nuclei, which helps electrons transfer from the adjacent C to N atoms, and N backdonates electrons.[42] Other factors may affect the ORR activities of N-doped carbons, for examples, the presence or absence of transition metals and the catalyst morphologies.[43] While, the different morphologies of rGFe-800a and GFe-800a might also exert influence on the catalytic activity (Figure S6). The rGFe-800a sample derived from the rGFe, should process a relatively large specific surface area due to the intercalation of the Fe nanoparticles formed in the process of pyrolysis (Table 1). Therefore, the restacking of graphene in the case of rGFe-800a can be avoided, which allows the active sites residing on the graphene surface to be more easily accessible to O_2, and thus contribute much positively to the ORR activities.[44-47] On the contrary, GFe-800a sample was obtained from GFeCp containing a large amount of the stripped graphene sheets with thickness of around 17 nm. As expected, such a kind of carbon source would not be beneficial to achieving a high surface area for GFe-800a in the process of pyrolysis, therefore it is reasonable to believe that the active surface in GFe-800a would be smaller than that of rGFe-800a (Table 1).

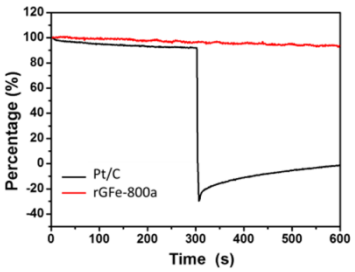

Figure 6. Chronoamperometric responses in O_2-saturated 0.1 M KOH after addition (at 300 second) of 2% (v/v) methanol for rGFe-800a (red line) and Pt/C (black line) electrocatalysts at -0.4 V.

We further measured the electrocatalytic selectivity of rGFe-800a and Pt/C against the electro-oxidation of methanol for the ORR, as shown in Figure 7. After the addition of 2% (v/v) methanol, the ORR current for rGFe-800a was almost unchanged, while Pt/C showed a sharp decrease, and even exhibited negative current. Hence, rGFe-800a indeed has a high selectivity for methanol, and enable effectively avoiding crossover effects, superior to the commercially available Pt/C catalyst in this aspect.

Conclusions

In this work, using ligand-exchange reaction of ferrocene and reduced graphene oxide, CpFe-modifed reduced graphene oxide (rGFeCp) was readily obtained. This method can be further used for exfoliation of graphite into multilayer graphene, and meanwhile formation of CpFe-modified multilayer graphene (GFeCp) in a simply one-pot performance. The as-produced iron(II) GFeCp exhibit good processability in most of organic solvents. After pyrolysis and ammonia activation under 800 ℃, 2D iron/nitrogen co-doped porous graphene or graphite (rGFe-800a or GFe-800a) were produced. As a non-precious metal catalyst for oxygen reduction reaction (ORR), rGFe-800a exhibited good electrochemical performance under alkaline condition (0.1 M KOH), with a low half-wave potential of -0.29 V, a dominant four-electron transfer mechanism (n=3.5 at -1.0 V) and a maximum diffusion-

limiting current density of 4.86 mAcm^{-2}. Meanwhile, it exhibited high methanol tolerance, superior to commercial 20% Pt/C. These characters of rGFe-800a manifested that the iron/nitrogen co-doping effect enable efficiently improving the ORR catalytic activity of graphene-based materials, which might provide a new way to developing composite materials with potentially practical applications in fuel cells and metal-air batteries. And taking advantage of ferrocene as a dual role of either intercalator or functional reactant for the exfoliation of graphite into the graphene nanosheets modified with CpFe moieties, might represent efficiently low-cost and green preparation of the functional graphene materials in large-scale.

Acknowledgements

This work was financially supported by the National Basic Research Program of China (973 Program: 2013CBA01602, 2012CB933404), the Natural Science Foundation of China (21174083, 51403126 and 21102091), the Shanghai Pujiang Program (12PJ1405300), and Shanghai Jiao Tong University (211 Project), the Ph.D. Programs Foundation of the Ministry of Education of the People's Republic China for Young Scholars (20110073120039).

Notes and references

[a] School of Mechanical and Power Engineering & Institute of Nuclear Technology and Application, East China University of Science and Technology, Shanghai, 200237, China
E-mail: (Z. L.) lizhi69@yeah.net; (B. L.) binlee@ecust.edu.cn
[b] School of Chemistry and Chemical Engineering, Shanghai Jiao Tong University,800 Dongchuan Road, Shanghai 200240, China
E-mail: (F. Z.) fan-zhang@sjtu.edu.cn
[c] Technische Universitaet Dresden, 01062 Dresden, Germany.
† These two authors contributed equally to this work.

Electronic Supplementary Information (ESI) available: Preparation details, TGA spectra, AFM image, XPS survey, XRD spectra and ORR performance of GFe-800a, elemental analysis based on XPS analysis. See DOI: 10.1039/c000000x/

1. F. Li, J. Song, H. Yang, S. Gan, Q. Zhang, D. Han, A. Ivaska and L. Niu, *Nanotechnology*, 2009, **20**, 455602.
2. S. Stankovich, D. A. Dikin, G. H. Dommett, K. M. Kohlhaas, E. J. Zimney, E. A. Stach, R. D. Piner, S. T. Nguyen and R. S. Ruoff, *Nature*, 2006, **442**, 282.
3. K. S. Novoselov, A. K. Geim, S. V. Morozov, D. Jiang, M. I. Katsnelson, I. V. Grigorieva, S. V. Dubonos and A. A. Firsov, *Nature*, 2005, **438**, 197.
4. T. Hasell, C. D. Wood, R. Clowes, J. T. A. Jones, Y. Z. Khimyak, D. J. Adams and A. I. Cooper, *Chem. Mater.*, 2010, **22**, 557
5. Y. Shi, K. K. Kim, A. Reina, M. Hofmann, L.J. Li and J. Kong, *ACS Nano*, 2010, **4**, 2689.
6. X. Wang, L. Zhi and K. Mullen, *Nano Lett.*, 2007, **8**, 323.
7. C. Zhang, R. Hao, H. Liao, Y. Hou, *Nano Energy*, 2013, **2**, 88.
8. B. Wang, *J. Power Sources*, 2005, **152**, 1.
9. V. Stamenković, T. J. Schmidt, P. N. Ross and N. M. Marković, *J. Electroanal. Chem.*, 2003, 554–555, 191.
10. S. Gottesfeld and T. A. Zawodzinski, Advances in Electrochemical Science and Engineering, Wiley-VCH, 2008, 195.
11. E. Antolini, T. Lopes and E. R. Gonzalez, *J. Alloys Compd.*, 2008, **461**, 253.
12. C. Cao, X. Zhuang, Y. Su, Y. Zhang, F. Zhang, D. Wu and X. Feng, Polym. Chem., 2014, 5, 2057.
13. J. Yang, D.-J. Liu, N. N. Kariuki and L. X. Chen, *Chem. Commun*, 2008, **3**, 329.
14. S. Yang, L. Zhi, K. Tang, X. Feng, J. Maier and K. Müllen, *Adv. Funct. Mater*, 2012, **22**, 3634.
15. D. Wei, Y. Liu, Y. Wang, H. Zhang, L. Huang and G. Yu, *Nano Lett*, 2009, **9**, 1752.
16. C. G. Lee, X. D. Wei, J. W. Kysar, J. Hone, *Science*, 2008, **321**, 385.
17. K. Gong, F. Du, Z. Xia, M. Durstock and L. Dai, Science, 2009, **323**, 760.
18. L. S. Panchakarla, A. Govindaraj and C. N. R. Rao, *ACS Nano*, 2007, **1**, 494.
19. J. Zhang, X. Liu, R. Blume, A. Zhang, R. Schlögl and D. S. Su, *Science*, 2008, **322**, 73.
20. F. Cheng and J. Chen, *Chem. Soc. Rev*., 2012, **41**, 2172.
21. Z. Chen, D. Higgins, A. Yu, L. Zhang and J. Zhang, *Energy & Environ. Sci*., 2011, **4**, 3167.
22. Q. Liu, H. Zhang, H. Zhong, S. Zhang and S. Chen, *Electrochim. Acta*, 2012, **81**, 313.
23. I. C. Liu, H.-M. Huang, C.-Y. Chang, H.-C. Tsai, C.-H. Hsu and R. C.-C. Tsiang, *Macromolecules*, 2003, **37**, 283.
24. L. Fan, Q. Zhang, K. Wang, F. Li and L. Niu, *J. Mater. Chem.*, 2012, **22**, 6165.
25. Y. Liang, Y. Li, H. Wang, J. Zhou, J. Wang, T. Regier and H. Dai, *Nat. Mater*., 2011, **10**, 780.
26. L. Zhang, J. Xia, Q. Zhao, L. Liu and Z. Zhang, *Small*, 2010, **6**, 537.
27. X. Wan, G. Long, L. Huang and Y. Chen, *Adv. Mater.*, 2011, **23**, 5342.
28. Q. Li, N. Mahmood, J. Zhu, Y. Hou, S. Sun, *Nano Today*, 2014, **9**, 668.
29. H. Yin, C. Zhang, F. Liu, Y. Hou, *Adv. Funct. Mater*. 2014, **24**, 2930.
30. W. H. Morrison, E. Y. Hou and D. N. Hendrickson, *J. Am. Chem. Soc.*, 1974, **96**, 3603.
31. N. Tsubokawa, N. Abe, G. Wei, J. Chen, S. Saitoh and K. Fujiki, *Polym. Chem*., 2002, **40**, 1868.
32. D. R. Dreyer, S. Park, C. W. Bielawski and R. S. Ruoff, *Chem. Soc. Rev*., 2010, 39, 228.
33. X. Huang, X. Qi, F. Boey and H. Zhang, *Chem. Soc. Rev*., 2012, **41**, 666.
34. Z.-H. Sheng, L. Shao, J.-J. Chen, W.-J. Bao, F.-B. Wang and X.-H. Xia, *ACS Nano*, 2011, **5**, 4350.
35. S. Chatrchyan, V. Khachatryan, A. M. Sirunyan, A. Tumasyan, W. Adam, T. Bergauer, M. Dragicevic, J. Erö, C. Fabjan and M. Friedl, *Phys. Rev. Lett*., 2011, **107**, 221804.
36. Z. Li, H. Chen, H. Bao and M. Gao, *Chem. Mater*., 2004, **16**, 1391.
37. P. Mills and J. L. Sullivan, J. Phys. D: *Appl. Phys*., 1983, **16**, 723.
38. L. Qu, Y. Liu, J.-B. Baek and L. Dai, *ACS Nano*, 2010, **4**, 1321.
39. B. C. H. Steele and A. Heinzel, *Nature*, 2001, **414**, 345.
40. R. Liu, D. Wu, X. Feng and K. Müllen, *Angew. Chem. Int. Ed*., 2010, **122**, 2619.
41. H. Kim, K. Lee, S. I. Woo and Y. Jung, *Phys. Chem. Chem. Phys*., 2011, **13**, 17505.

42. D. Deng, X. Pan, L. Yu, Y. Cui, Y. Jiang, J. Qi, W.-X. Li, Q. Fu, X. Ma, Q. Xue, G. Sun and X. Bao, *Chem. Mater*., 2011, **23**, 1188.
43. G. Wu, K. L. More, C. M. Johnston and P. Zelenay, *Science*, 2011, **332**, 443.
44. Z. S. Wu, L. Chen, J. Liu, K. Parvez, H. Liang, J. Shu, H. Sachdev, R. Graf, X. Feng and K. Müllen, *Adv. Mater.* 2013, **26**, 1450.
45. Z. S. Wu, S. B. Yang, Y. Sun, K. Parvez, X. L. Feng and K. Müllen, *J. Am. Chem. Soc.* 2012, **134**, 9082.
46. Z.S. Wu, W. Ren, L. Gao, B. Liu, C. Jiang and H.M. Cheng, *Carbon*, 2009, **47**, 493.
47. Z. S. Wu, W. Ren, L. Gao, J. Zhao, Z. Chen, B. Liu, D. Tang, B. Yu, C. Jiang and H. M. Cheng, *ACS Nano*, 2009, **3**, 411.

